Cloud Clusters, Kelvin Wave–CISK, and the Madden–Julian Oscillations in the Equatorial Troposphere

HAN-RU CHO

Department of Physics, University of Toronto, Toronto, Ontario, Canada

KLAUS FRAEDRICH

Meteorologisches Institut, Universität Hamburg, Hamburg, Germany

J. T. WANG

Institute of Atmospheric Physics, National Central University, Chung-Li, Taiwan

(Manuscript received 11 January 1993, in final form 29 April 1993)

ABSTRACT

The Kelvin wave–CISK theory of the Madden–Julian oscillations in the tropical troposphere is reexamined by introducing a phase lag between the maximum cloud heating and the maximum convergence of the Kelvin wave. The study was motivated by the observations in the equatorial Pacific that clouds in the Kelvin waves are organized into westward propagating mesoscale cloud clusters. Since this phase lag depends on the propagation speed of the Kelvin waves, the waves become dispersive, and this leads to a favored growth of long waves. The results of this study suggest that the presence of organized mesoscale cloud systems needs to be parameterized directly into those climate models that cannot adequately describe their dynamics.

1. Introduction

Among the several theories proposed to explain the 30–50 day oscillations of the tropical troposphere, two appear to be related. Emanuel (1987) and Neelin et al. (1987) suggested the phenomenon is caused by a wind–evaporation feedback mechanism that modulates cumulus convection as the energy source for the oscillation. In a test using a simplified general circulation model, Neelin et al. showed that the peaks around 20–25-day period in the power spectra of the deviation fields of the tropical troposphere are considerably enhanced with the inclusion of wind–evaporation feedback. In another theory proposed by Chang and Lim (1988) and Lau and Peng (1987), Kelvin wave–CISK was suggested as the responsible mechanism. However, because of the nondispersive nature of Kelvin waves, results from linear analyses suggest a scale selection that favors waves of short wavelength, rather than long wavelength such as wavenumber 1 or 2, as required by the phenomenon.

Some authors attempted to find a solution to this scale selection problem by looking for processes that may suppress the rapid growth of Kelvin–CISK at short wavelength. Wang and Rui (1989, 1990), for example, showed by considering the coupling of Kelvin wave–CISK modes with the Rossby waves through Ekman-type boundary-layer effects, that the wave–CISK modes are most unstable at wavenumbers 1 or 2. A few others, such as Lau and Peng (1987) and Lim et al. (1990) on the other hand, argue that linear CISK analysis is inappropriate because negative heating is allowed in regions of downward motion. These authors demonstrated that the scale selection problem can be avoided altogether if a "positive-only nonlinear heating" is used to represent the cumulus effects. As explained in Lim et al., this "nonlinear effect" is present even when the amplitude of the disturbance is very small, and it is therefore a very severe form of nonlinearity. Using a model with a "positive-only nonlinear heating," but linearized in all other terms of the governing equations, Lim et al. showed that the Fourier components of a disturbance, after a period of initial adjustment, all grow at the same rate so that the form of the disturbance can be preserved. However, a recent analysis by Crum and Dunkerton (1992) seems to suggest that the scale selection problem in linear Kelvin wave–CISK theory is only modified by the introduction of nonlinear heating but not eliminated.

The purpose of this paper is to consider yet another aspect of this scale selection problem: namely, the organization of cumulus clouds into cloud clusters, and

Corresponding author address: Prof. Han-Ru Cho, University of Toronto, Department of Physics, Toronto, Ontario, Canada M5S 1A7.

the effect of this organization on the distribution of heating in the Kelvin wave. The study is partly motivated by the fact that the positions of cumulus convection in the Kelvin waves in the theories just mentioned do not appear to agree with observations. Qualitative results from observational studies seem to suggest that areas of strongest cumulus activities appear to the west (or, lagging in phase) of the region of low-level convergence (Nakazawa 1988; Madden and Julian 1971, 1972), while in the traditional linear wave–CISK theory or in "the nonlinear CISK" theory, it is assumed to take place in phase with low-level convergence. The location of cumulus convection in the wind–evaporation feedback theory depends on the direction of the background wind. If a low-level easterly wind is assumed in the background in accordance with the observed mean state of the equatorial troposphere, then cumulus convection should be the strongest to the east, in advance of the low-level convergence.

The observational evidence of a time lag between cumulus convection and low-level convergence was first reported by Cho and Ogura (1974); the effect of a time lag on the wave–CISK theory was first examined in Davies (1979), where the plausibility of the time lag was discussed. There are several physical processes that may cause a phase difference between low-level convergence and cumulus convection; one which has the potential to cause the longest phase delay is that cumulonimbi are often organized into mesoscale systems, which propagate at a velocity distinctly different from the background system in which they are embedded. Nakazawa (1988) recently reported a hierarchy of cloud organizations associated with the 30–60 day oscillations; the smallest unit is the westward propagating mesoscale cloud clusters embedded inside the synoptic-scale eastward propagating superclusters. The cloud clusters typically have a lifetime of about two days, and travel about 2000 km during their lifetimes, a fair distance even for global-scale systems. This observed hierarchical structure forms the basis of this study. A specific scheme will be proposed to incorporate the effect on the distribution of heating due to the westward propagation of the cloud clusters. We will show that, because of the phase lag in heating caused by the cloud clusters, even the linear wave–CISK theory may exhibit the necessary scale selection to remain a credible explanation for the Madden–Julian oscillations.

2. Governing equations and Kelvin waves

The governing equations for the Kelvin waves in the pressure coordinate system after linearization in the equatorial beta plane are

$$\frac{\partial u}{\partial t} + \frac{\partial \Phi}{\partial x} = 0 \tag{1a}$$

$$\frac{\partial \Phi}{\partial y} + \beta y u = 0 \tag{1b}$$

$$\frac{\partial u}{\partial x} + \frac{\partial \omega}{\partial p} = 0 \tag{1c}$$

$$\frac{\partial}{\partial t}\left(\frac{\partial \Phi}{\partial p}\right) + \sigma\omega = -\frac{\alpha}{C_p}\frac{ds}{dt} \tag{1d}$$

$$\frac{\partial \Phi}{\partial p} = -\alpha = -\frac{RT}{p}. \tag{1e}$$

The right-hand-side term of (1d) represents the heating rate due to cumulus convection where s is the entropy; σ in this equation is the stability parameter. The last of these equations is the hydrostatic relation where α is the specific volume, R the gas constant, and T the temperature.

If a sinusoidal dependence in x and t is assumed in the form

$$\exp[i(\mu t + kx)]$$

then the governing equations become

$$i\mu u + ik\Phi = 0 \tag{2a}$$

$$\frac{\partial \Phi}{\partial y} + \beta y u = 0 \tag{2b}$$

$$iku + \frac{\partial \omega}{\partial p} = 0 \tag{2c}$$

$$i\mu\left(\frac{\partial \Phi}{\partial p}\right) + \sigma\omega = Q. \tag{2d}$$

The term Q in (2d) represents the heating term on the right side of (1d). Eliminating u from (2a) and (2b), one obtains the solution:

$$\Phi = \Phi_0 \exp\left[-\frac{\beta}{2c} y^2\right], \tag{3}$$

where $c = -\mu/k$. Therefore, equatorially trapped solutions are possible only if the real part of c, $\mathrm{Re}(c) > 0$, or eastward propagating waves. The governing equations may be reduced to a single equation in terms of the vertical p velocity ω:

$$\frac{\partial^2 \omega}{\partial p^2} + \frac{\sigma}{c^2}\omega = \frac{1}{c^2}Q. \tag{4}$$

This is obtained from (2a), (2c), and (2d) by eliminating all other variables.

We will assume as in many CISK studies that the heating rate is proportional to low-level convergence, represented by the vertical velocity ω^* at a low-level $p = p^*$:

$$Q = \epsilon\sigma\omega^* f(p); \tag{5}$$

$f(p)$ here is a normalized vertical distribution function:

$$\frac{1}{\Delta p}\int_{p_t}^{p_s} f(p)dp = 1$$

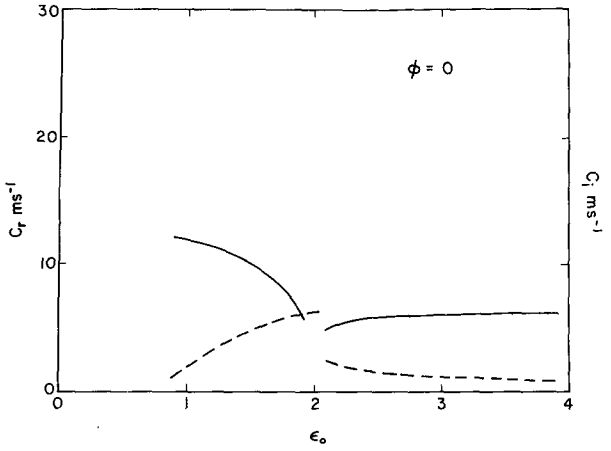

FIG. 1. The real (solid curves) and the imaginary (dashed curves) part of the complex propagation speed as functions of the heating parameter ϵ_0, for the piecewise linear heating profiles with zero phase lag. Only unstable modes with $c_i \geq 1$ m s^{-1} are shown.

where $\Delta p = (p_s - p_t)$, the difference between the pressures at the surface and at the tropopause, respectively. Here ϵ is a nondimensional constant indicating the intensity of heating. Later in this paper we will consider the effects of a phase difference between heating and low-level convergence, and this can be accomplished by letting ϵ have a complex value.

Equation (4) together with the heating parameterization gives rise to an eigenvalue problem in terms of c. Given the heating rate Q, (4) can be solved to give $\omega(p)$; but heating in turn depends on the vertical velocity ω. Therefore, the condition that

$$\omega(p^*) = \omega^*$$

gives rise to an equation that can be solved for the eigenvalue c.

3. Sinusoidal heating profile

Our interest in this problem was stimulated by the discovery that if a simple sinusoidal heating profile is assumed in (5), no unstable solution can be found if ϵ is assumed to be real. A simple calculation will verify this: assuming

$$f(p) = \frac{\pi}{2} \sin\left[\frac{\pi}{\Delta P}(p_s - p)\right], \tag{6}$$

(4) is satisfied by

$$\omega = \frac{\pi\epsilon\sigma\omega^*}{2\left(\sigma - c^2\left(\frac{\pi}{\Delta p}\right)^2\right)} \sin\left[\frac{\pi}{\Delta p}(p_s - p)\right]. \tag{7}$$

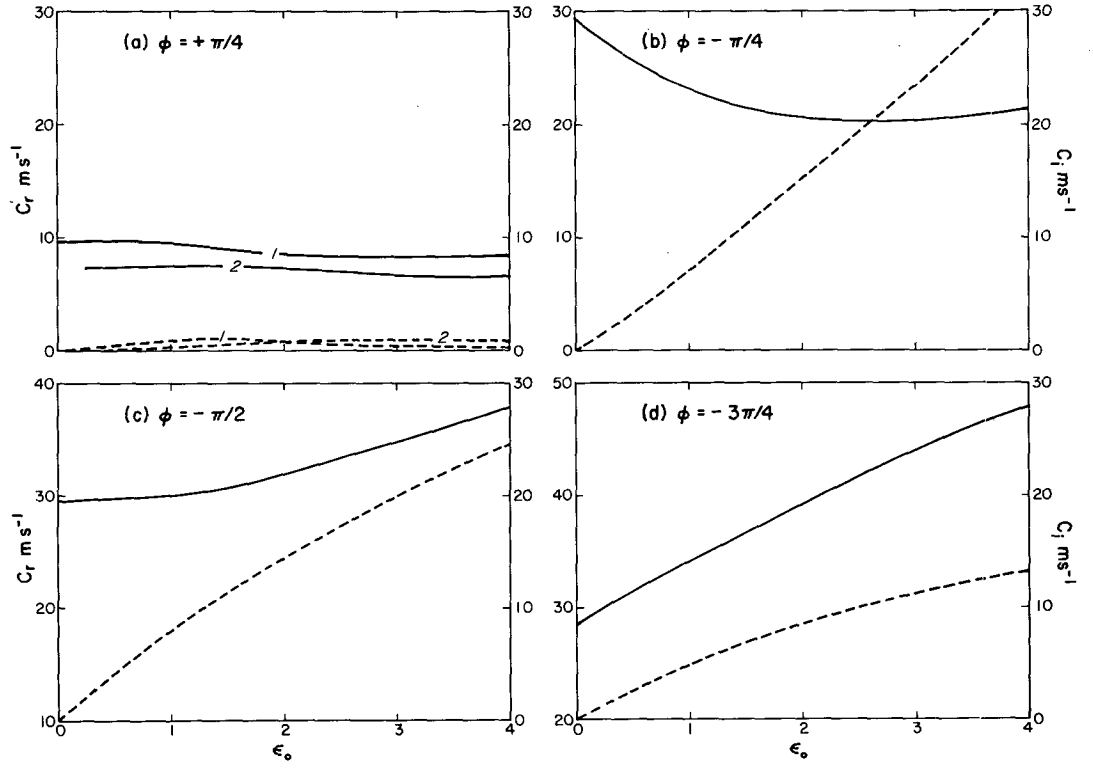

FIG. 2. Same as in Fig. 1 except a phase angle ϕ is introduced between maximum cloud heating and maximum low-level convergence: (a) $\phi = +\pi/4$, (b) $\phi = -\pi/4$, (c) $\phi = -\pi/2$, and (d) $\phi = -3\pi/4$. Negative phase angle indicates heating lagging behind low-level convergence.

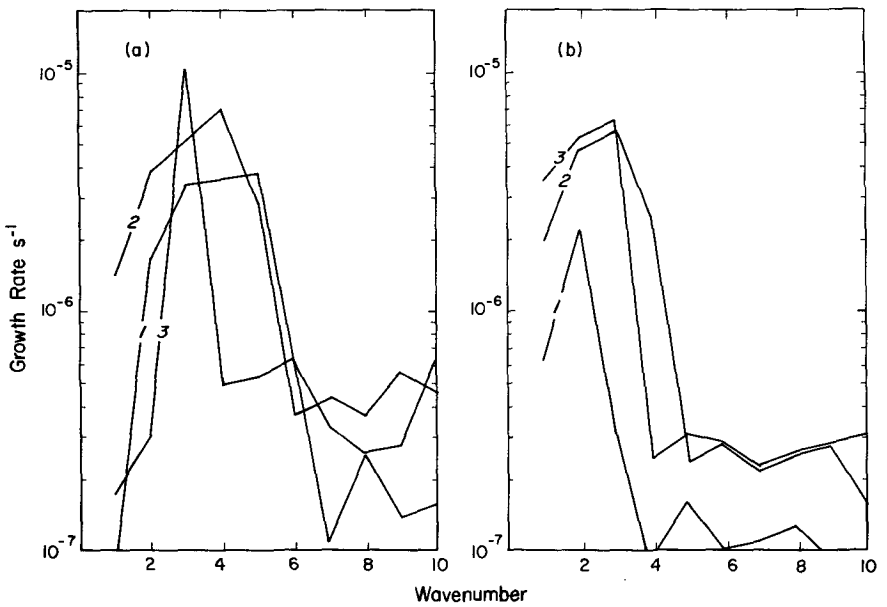

FIG. 3. Growth rates of Kelvin waves as a function of wavenumber when a phase angle is introduced according to (15). The vertical distribution of heating is piecewise linear, same as in Figs. 1 and 2. The curves labeled 1, 2, and 3 correspond to 1.0, 2.0, and 3.0 for the heating parameter ϵ_0. Panel (a) corresponds to the case $c_1 = 0.0$ m s^{-1} and panel (b) $c_1 = -10.0$ m s^{-1}. The calculations are made assuming the cloud clusters have a half-lifetime of 24 hours.

The condition that $\omega(p^*) = \omega^*$ requires

$$1 = \frac{\pi\epsilon\sigma}{2[\sigma - c^2(\pi/\Delta p)^2]} \sin\left[\frac{\pi}{\Delta p}(p_s - p^*)\right]$$

which gives

$$c = \pm \frac{\Delta p}{\pi} \sigma^{1/2}\left\{1 - \frac{\pi}{2}\epsilon \sin\left[\left(\frac{p_s - p^*}{\Delta p}\right)\pi\right]\right\}^{1/2}; \quad (8)$$

c is real or pure imaginary depending on the value of ϵ, so long as it is a real number. The pure imaginary value of c is obtained when

$$\epsilon > \epsilon_c = 2 \Big/ \pi \sin\left[\left(\frac{p_s - p^*}{\Delta p}\right)\pi\right],$$

that is, when cumulus heating is greater than adiabatic cooling at all height levels. This represents an unstable mode. However, according to (3), a pure imaginary value of c does not represent an equatorially trapped wave; therefore it is not a physically realistic solution. Assuming

$$p_s = 1000 \text{ mb}, \quad p_t = 100 \text{ mb}, \quad p^* = 900 \text{ mb}$$

the critical value of ϵ is

$$\epsilon_c = 1.87.$$

For $\epsilon < \epsilon_c$ we have only stable solutions. Assuming 10^{-6} for the value of σ, we have

$$c \approx 30\left(1 - \frac{\epsilon}{\epsilon_c}\right)^{1/2}.$$

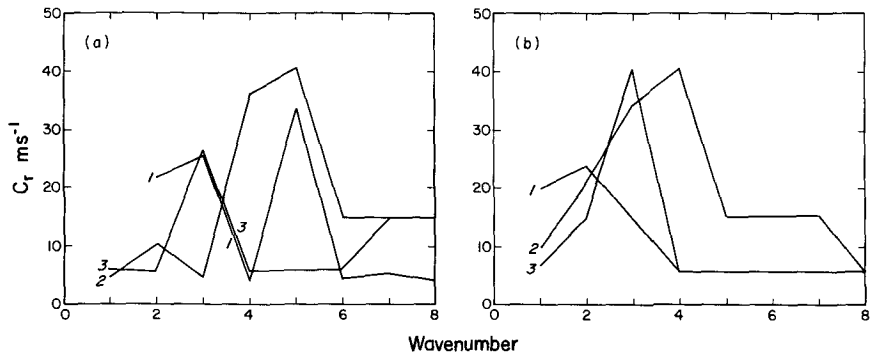

FIG. 4. The phase speeds of the Kelvin waves corresponding to cases shown in Fig. 3.

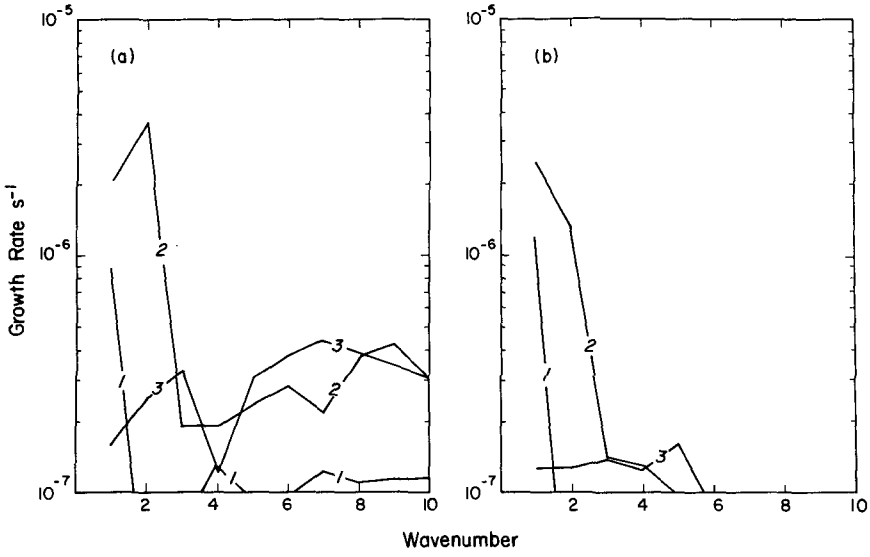

FIG. 5. Same as in Fig. 3 except the half-lifetime for the cloud clusters is assumed to be 48 hours.

Results from observational studies seem to suggest that in general the strongest cumulus convection does not always occur at the place where we have the largest low-level convergence (e.g., Cho and Ogura 1974). This difference in phase between cumulus heating and low-level convergence can be accommodated by allowing ϵ to have complex values; as can be seen from (5), the phase angle of a complex ϵ corresponds to a phase shift between the heating and the low-level convergence of a linear sinusoidal wave. It is easy to see from (8) that physically acceptable unstable mode is possible in this situation. The effect of this phase shift will be discussed in detail later in this paper.

4. Piecewise linear heating profile

In more general cases unstable solutions are possible even for real values of ϵ. We consider, for example, a piecewise linear heating profile given by

$$f(p) = \begin{cases} \dfrac{2(p_s - p)}{(p_s - p_p)}, & p > p_p \\ \dfrac{2(p - p_t)}{(p_p - p_t)}, & p_p \geqslant p, \end{cases} \tag{9}$$

where p_p is the level of maximum heating. To obtain the solution of this eigenvalue problem, we write

$$\omega = \omega_p + \omega_c$$

and let

$$\omega_p = \epsilon\omega^* f(p).$$

Since

$$\frac{d^2\omega_p}{dp^2} + \frac{\sigma}{c^2}\omega_p = \frac{1}{c^2}Q - \frac{2\epsilon\omega^*(p_s - p_t)}{(p_s - p_p)(p_p - p_t)}\delta(p - p_p),$$

where δ is the Dirac delta function, we require

$$\frac{d^2\omega_c}{dp^2} + \frac{\sigma}{c^2}\omega_c = \frac{2\epsilon\omega^*(p_s - p_t)}{(p_s - p_p)(p_p - p_t)}\delta(p - p_p) \tag{10}$$

subject to the boundary condition that $\omega_c = 0$ at $p = p_s$ and $p = p_t$. It is straightforward to show that

$$\omega_c = \frac{2\epsilon\omega^*(p_s - p_t)}{(p_s - p_p)(p_p - p_t)} G(p, p_p),$$

where $G(p, p_p)$ is the Green function (see Appendix)

$$G(p, p_p) = \begin{cases} \dfrac{c}{N}\dfrac{\sin\left[\dfrac{N}{c}(p_p - p_c)\right]\sin\left[\dfrac{N}{c}(p - p_s)\right]}{\sin\left[\dfrac{N}{c}(p_p - p_t)\right]}, \\ \qquad\qquad p_s > p > p_p \\ \dfrac{c}{N}\dfrac{\sin\left[\dfrac{N}{c}(p_p - p_s)\right]\sin\left[\dfrac{N}{c}(p - p_t)\right]}{\sin\left[\dfrac{N}{c}(p_s - p_t)\right]}, \\ \qquad\qquad p_p > p > p_t; \end{cases} \tag{11}$$

N here is used to denote

$$N = \sqrt{\sigma}.$$

Combining ω_c and ω_p, one obtains

$$\omega = \epsilon\omega^* f(p) + \frac{2\epsilon\omega^*(p_s - p_t)}{(p_s - p_p)(p_p - p_t)} G(p, p_p). \tag{12}$$

Now, usually $p^* > p_p$, the condition that $\omega = \omega^*$ at $p = p^*$ gives the following equation,

$$g(c) = 1 - \frac{2\epsilon(p_s - p^*)}{(p_s - p_p)} - \frac{c}{N}\frac{2\epsilon(p_s - p_t)}{(p_s - p_p)(p_p - p_t)}\frac{\sin\left[\frac{N}{c}(p_p - p_t)\right]\sin\left[\frac{N}{c}(p^* - p_s)\right]}{\sin\left[\frac{N}{c}(p_s - p_t)\right]} = 0. \quad (13)$$

It is difficult to find solutions of this eigenvalue equation by analytic means. Instead, a numerical method is used to determine the zeros of $g(c)$. For $c = c_r + ic_i$, where c_r and c_i are the real and imaginary values of c, the values of g are scanned in the region $0 < c_r \leq 50$ and $0 \leq c_i \leq 50$, with intervals Δc_r and Δc_i 0.1 m s^{-1}. A particular interval is considered to contain a zero if both the real part and the imaginary part of g change their signs over the interval. Note that this method will find only eastward-propagating neutral and unstable modes. The following values for the parameters are used:

$$p_s = 1000 \text{ mb}, \quad p_t = 100 \text{ mb},$$
$$p_p = 600 \text{ mb}, \quad \sigma = 10^{-6}.$$

Figure 1 shows the unstable modes determined using this method as functions of ϵ in the range (0, 4). Several unstable modes are found, but only those with $\max(c_i) \geq 1$ m s^{-1} are shown in this as well as the following figures. The solid line shows the real part of c and the dashed line the imaginary part. Here c_r ranges between 6 and 12 m s^{-1}, while c_i has values 1–6 m s^{-1}. As a reference for comparison, it is noted that a wave with phase speed $c_r = 10$ m s^{-1} travels around the earth in about 42 days. For a given value of c_i, the growth rate of the wave is inversely proportional to wavelength because of the nondispersive nature of the Kelvin wave. For $c_i = 1$ m s^{-1}, the e-folding time for waves with wavelength $\lambda = 1000$ km is about 1.9 days, while the corresponding e-folding time for wavenumber 1 wave is 69 days. This represents a considerable weakness for the Kelvin wave–CISK theory: the CISK mechanism appears to favor the growth of waves with short wavelength instead of waves of global extent.

The role of the phase difference between wave-induced low-level convergence and heating can be examined by letting

$$\epsilon = \epsilon_0 \exp(i\phi). \quad (14)$$

Positive or negative values of the phase angle ϕ correspond to the positions of cumulus heating leading or lagging in phase relative to the wave-induced low-level convergence. The real and imaginary parts of the eigenvalues as functions of ϵ_0 are shown in Fig. 2 for (a) $\phi = \pi/4$, (b) $\phi = -\pi/4$, (c) $\phi = -\pi/2$, and (d) $\phi = -3\pi/4$. Again eigenmodes with $\max(c_i) < 1$ m s^{-1} are not shown in these diagrams. For the same value of ϵ_0 the phase speed of the most unstable wave increases as ϕ decreases from $\pi/4$ to $-3\pi/4$. Note the axis for c_r has been shifted downward by 10 m s^{-1} for $\phi = -\pi/2$, and by 20 m s^{-1} for $\phi = -3\pi/4$. The imaginary part of c first increases, then decreases with decreasing values of ϕ. For $\epsilon_0 = 2$ and $\phi = -\pi/4$, for example, the most unstable mode has $c_i = 15$ m s^{-1}, or an e-folding time of 4.6 days for a wave with wavelength equal to circumference of the earth at the equator. But because of the nondispersive nature of Kelvin waves, the shortest wave grows the fastest.

5. Incorporating the propagating cloud clusters

One of the main differences between the air–sea interaction theory according to Neelin et al. (1987) and Emanuel (1987) and the Kelvin wave–CISK theory is the relative location of cumulus heating in the disturbance. If the surface evaporation is included as a moisture source in addition to low-level convergence, the relative location of cumulus heating will be shifted from the position of maximum low-level convergence toward the position of maximum surface evaporation. Since in a linear normal-mode analysis the magnitudes of the variables are proportional to one another, one can assume cumulus heating to be proportional to any of the disturbance variables provided an appropriate phase angle is taken into account.

In a recent observational analysis using GMS high-resolution IR data, Nakazawa (1988) showed a hierarchy of organizations of cumulus convection in the 30–50 day oscillations in the equatorial western Pacific. The oscillation is associated with a number of synoptic-scale super cloud clusters that have a horizontal scale of several thousand kilometers and propagate eastward at a speed about equal to that of the Madden–Julian oscillations. Within each super cloud cluster are short-lived cloud clusters with a typical lifetime of the order of two days. These clusters are typically generated in the region of low-level convergence, but propagate westward at a speed about 10 m s^{-1} to the rear of a super cloud cluster.

The presence of propagating cloud clusters suggests that the location of maximum cloud heating is not likely to be at the place where the clusters are generated. Since the propagation speed of the super cloud clusters is about the same as the propagation speed of the Madden–Julian oscillations, they are not likely to contribute to any significant phase shift between low-level convergence and cloud heating. The westward propagating

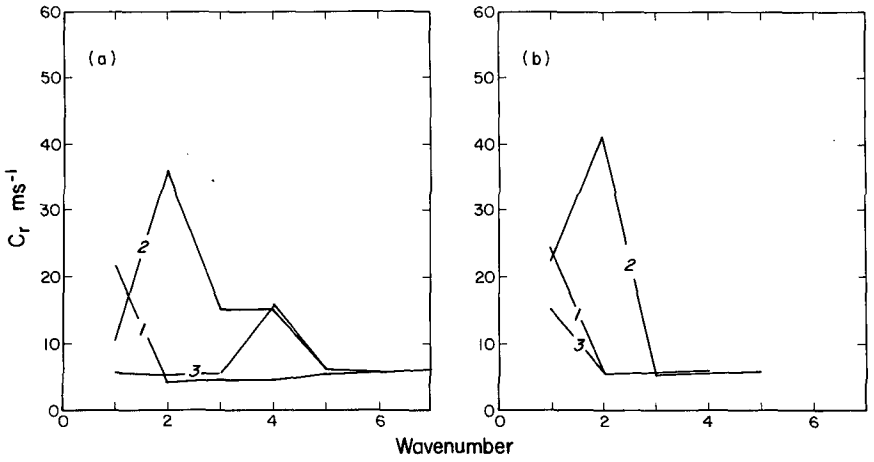

FIG. 6. Phase speeds of the Kelvin waves corresponding to cases shown in Fig. 5.

cloud clusters, however, will be able to cause considerable phase shift if heating maxima are not reached during the early stages of their lifetimes. If one assumes the heating maximum is reached at the half lifetime of a cloud cluster, then the following phase shift between low-level convergence and heating can be expected:

$$\phi = \frac{\tau}{2}(c_1 - c_r)k, \qquad (15)$$

where τ is the mean lifetime of the cloud clusters and c_1 its propagation speed; c_r and k are the real part of the phase speed and the wavenumber of the Kelvin wave. In our calculations we have imposed the condition that $-\pi < \phi < \pi$, for otherwise we would be allowing the unrealistic situation to happen where the cloud clusters are allowed to propagate over one wavelength in either the positive or the negative direction. The introduction of such a phase shift in cumulus heating means the parameterized heating is dependent on both the phase speed as well as the wavenumber of the wave; consequently, the Kelvin wave becomes dispersive.

a. Piecewise linear heating profile

We first consider the case of a piecewise linear heating profile. The CISK analysis with a phase shift given by (15) is performed in the same way as described in the previous section. Figure 3 shows the growth rate (instead of the imaginary part of the phase speed) as a function of wavenumber. The calculations are done with $\tau/2 = 24$ h; all other parameters are the same as described before. Panel (a) shows the results obtained with $c_1 = 0$, while panel (b) is for the case with $c_1 = -10$ m s^{-1}. The lines labeled 1, 2, and 3 in each panel correspond to the values of the heating parameter $\epsilon_0 = 1$, 2, and 3. Results shown in these panels indicate that the growth rates have maxima toward the long wavelength end of the spectra. The peaks in growth rates in the case $c_1 = 0$ m s^{-1} are located at wavenumbers 3, 4, or 5, depending on the value of the heating parameter. In all three cases, however, the growth rate drops rapidly toward wavenumber 1. In the case $c_1 = -10$ m s^{-1}, the growth rate peaks at wavenumber 2 when $\epsilon_0 = 1.0$, with much smaller growth rates at both wavenumbers 1 and 3. For $\epsilon_0 = 2.0$ or 3.0, the peaks are located at wavenumber 3, but the scale selection is weak among the first three wavenumbers of the spectra.

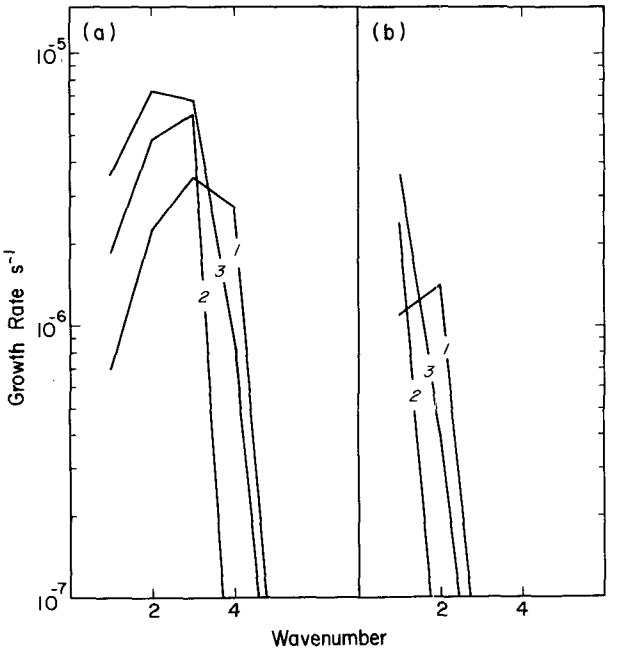

FIG. 7. Growth rates of Kelvin waves when a sine heating profile is used. A phase angle between heating and wave convergence is introduced according to (15), as in Fig. 3. The results shown are for the cases $c_1 = -10.0$ m s^{-1}: (a) $\tau/2 = 24$ hours and (b) $\tau/2 = 48$ hours. Labels 1, 2, and 3 are the same as in Fig. 3.

The maximum growth rates in these two cases are about 0.6 day^{-1}.

Although the present analysis assumes no background wind, it can be considered as carried out in a moving reference frame provided that the background wind is uniform with height. Therefore, it is somewhat difficult to decide what phase speeds for the Kelvin waves are implied by the periods of the Madden–Julian oscillations. For Kelvin waves with wavenumber equal to 1, 30–50 day periods correspond to phase speeds 7–12 m s^{-1}. But considering the Doppler effect of the mean easterly wind over the equatorial region, a phase speed anywhere between 7 and 25 m s^{-1} can probably be considered as reasonable.

The phase speeds of the waves obtained in this analysis are shown in Fig. 4 for (a) $c_1 = 0$ and (b) $c_1 = -10$ m s^{-1}. In the first case, $c_1 = 0$ m s^{-1}, the phase speeds for waves with wavenumbers 1, 2, and 3 are all within reasonable range. But the phase speeds are probably too large at wavenumber 4 for $\epsilon_0 = 2.0$, and at wavenumber 5 for $\epsilon_0 = 1.0$ and 2.0. In the case $c_1 = -10$ m s^{-1}, the phase speeds are reasonable at wavenumber 1 and 2 for all three values of ϵ_0. At wavenumber 3, the phase speeds exceed 30 m s^{-1} for $\epsilon_0 = 2.0$ and 3.0.

We have repeated the analysis using $\tau/2 = 2$ days. The results are shown in Fig. 5 for the growth rate spectra and in Fig. 6 for the phase speeds of the Kelvin waves. In both of the cases $c_1 = 0$ m s^{-1} and $c_1 = -10$ m s^{-1}, the growth rates at $\epsilon_0 = 3.0$ are very small at all wavenumbers shown. At $\epsilon_0 = 1.0$ and 2.0, the spectra are much narrower than those obtained with $\tau/2 = 1$ day, and have peaks located at wavenumbers 1 and 2. The *e*-folding times at maximum growth rate for $\epsilon_0 = 2.0$ are about 3 days when $c_1 = 0.0$ m s^{-1}, and 4 days for $c_1 = -10.0$ m s^{-1}.

b. Sine heating profile

A similar analysis was also carried out using the sine heating profile given in (6). The results are very similar to those described in the previous subsection: maxima are found in the long wavelength end of the growth rate spectra for the variety of values of the background parameters specified. Figure 7 shows as an example the growth rate of the Kelvin wave as a function of the wavenumber for the cases with $c_1 = -10$ m s^{-1}, and $\tau/2$ equals (a) 24 h and (b) 48 h. Note that in these cases no growth was found for the waves with wavelength shorter than that of wavenumber 4.

6. Discussion and conclusions

An alternative to the nonlinear Kelvin wave–CISK theory (Lim et al. 1990) is proposed to overcome the scale selection problem in traditional linear Kelvin wave–CISK analysis. The analysis is based on the observations that in the equatorial Pacific, cumulus clouds are organized into westward propagating cloud clusters, which in turn are organized into superclusters that propagate at about the same phase speed as the Kelvin waves in which they are embedded. We attempt to parameterize the presence of this hierarchical structure in terms of a phase lag between the low-level convergence and the maximum cloud heating. This phase lag depends on the phase speed of the background Kelvin wave and the speed of the cloud clusters, and as a result the Kelvin wave becomes dispersive, leading to the preferred long-wave growth. In a qualitative sense this can be visualized as organized cloud clusters commencing their activities at a maximum of low-level convergence, propagating westward, and reaching maximum heating at about half-life time. It is in agreement with the observations that clouds appear mostly to the west of the low-level convergence in equatorial Kelvin waves.

The results of this study appear to suggest the following.

1) Cumulus convection does not lead directly to the presence of the Madden–Julian oscillations. Instead, they are organized into cloud clusters that are meso-α-scale phenomenon.

2) The Madden–Julian oscillations are caused by latent heat release in organized cloud clusters.

3) Therefore, the observed hierarchical organization of cloud clusters should be considered as an integral part of the dynamical processes leading to the 30–50 day oscillations of the tropical troposphere.

Among the theories that have been proposed to explain the 30–50 day oscillations, only the process proposed in this study and that discussed in Wang and Rui (1989, 1990) show the correct scale selection property. The Kelvin waves in the wind–evaporation feedback theory discussed in Neelin et al. (1987) and Emanuel (1987), as in the original Kelvin wave–CISK theory (Lau and Peng 1987; Chang and Lim 1988), are nondispersive and therefore are most unstable at the shortest wavelength. A recent study by Crum and Dunkerton (1992) suggested that even the nonlinear effect in the "positive-only nonlinear heating" (Lau and Peng 1987; Lim et al. 1990) only modified but did not eliminate this scale selection problem. It would be interesting in the future to construct a model that allows us to select and combine these processes, and to compare the model results with observations in order to narrow the range of possible explanations of the Madden–Julian oscillations.

In addition, we did not consider in this study the presence of superclusters. What are the effects of super clusters on the Madden–Julian oscillations? What are the processes responsible for the organizations of clouds into clusters and superclusters? These are but a few of the questions that must be addressed in order to understand the complete dynamical processes leading to the appearance of the 30–50 day oscillations in the tropical troposphere.

Acknowledgments. The research was supported in part by research grants from the Canadian Natural Sciences and Engineering Research Council, the Atmospheric Environment Service of Canada, and the Federal Ministry of Science and Technology of Germany. The work was initiated when one of us (HRC) was visiting the National Central University under the sponsorship of the National Science Council of Taiwan.

APPENDIX

The Green Function

We will use p_p^+ to denote the limiting value of p when it approaches p_p from the side where $p > p_p$, and p_p^- from the $p < p_p$ side. To determine the Green function given in (11), we note the $G(p, p_p)$ in the solution of ω_c can be written as

$$G(p, p_p) = \begin{cases} A \sin\left[\dfrac{N}{c}(p - p_s)\right], & p_s > p > p_p \\ B \sin\left[\dfrac{N}{c}(p - p_t)\right], & p_p > p > p_t. \end{cases}$$

From this expression the derivative of $G(p, p_p)$ with respect to p can be determined easily:

$$\frac{dG(p, p_p)}{dp} = \begin{cases} A \dfrac{N}{c} \cos\left[\dfrac{N}{c}(p - p_s)\right], & p_s > p > p_p \\ B \dfrac{N}{c} \cos\left[\dfrac{N}{c}(p - p_t)\right], & p_p > p > p_t. \end{cases}$$

By definition, G should be continuous across p_p, while its derivative is discontinuous with a jump from p_p^+ to p_p^- equal to unity:

$$A \sin\left[\frac{N}{c}(p_p - p_s)\right] - B \sin\left[\frac{N}{c}(p_p - p_t)\right] = 0$$

$$A \frac{N}{c} \cos\left[\frac{N}{c}(p_p - p_s)\right] - B \frac{N}{c} \cos\left[\frac{N}{c}(p_p - p_t)\right] = 1.$$

These equations can be solved for A and B to give the Green function given in (11).

REFERENCES

Chang, C. P., and H. Lim, 1988: Kelvin wave-CISK: A possible mechanism for the 30–50 day oscillations. *J. Atmos. Sci.*, **45,** 1709–1720.

Cho, H. R., and Y. Ogura, 1974: A relationship between cloud activity and the low-level convergence as observed in Reed–Recker's composite easterly waves. *J. Atmos. Sci.*, **31,** 2058–2065.

Crum, F. R., and T. J. Dunkerton, 1992: Analytic and numerical models of wave-CISK with conditional heating. *J. Atmos. Sci.*, **49,** 1693–1708.

Davies, H. C., 1979: Phase-lagged wave-CISK. *Quart. J. Roy. Meteor. Soc.*, **105,** 323–353.

Emanuel, K. A., 1987: An air–sea interaction model of intraseasonal oscillations in the tropics. *J. Atmos. Sci.*, **44,** 2324–2340.

Lau, K. M., and L. Peng, 1987: Origin of low-frequency (intraseasonal) oscillations in the tropical atmosphere. Part I: Basic theory. *J. Atmos. Sci.*, **44,** 950–972.

——, ——, C. H. Sui, and T. Nakazawa, 1989: Dynamics of super clusters, wind bursts, 30–60 day oscillations and ENSO: A unified view. *J. Meteor. Soc. Japan,* **67,** 205–219.

Lim, H., T. K. Lim, and C. P. Chang, 1990: Reexamination of wave-CISK theory: Existence and properties of nonlinear wave-CISK modes. *J. Atmos. Sci.*, **47,** 3078–3091.

Madden, R., and P. R. Julian, 1971: Detection of a 40–50 day oscillation in the zonal wind in the tropical Pacific. *J. Atmos. Sci.*, **28,** 702–708.

——, and ——, 1972: Description of global circulation cells in the tropics with a 40–50 day period. *J. Atmos. Sci.*, **29,** 1109–1123.

Nakazawa, T., 1988: Tropical super clusters within intraseasonal variations over the Western Pacific. *J. Meteor. Soc. Japan,* **66,** 823–839.

Neelin, J. D., I. M. Held, and K. H. Cook, 1987: Evaporation-wind feedback and low-frequency variability in the tropical atmosphere. *J. Atmos. Sci.*, **44,** 2341–2348.

Sui, C. H., and K. M. Lau, 1989: Origin of low-frequency (intraseasonal) oscillations in the tropical atmosphere. Part II: Effect of an improved treatment of moist processes. *J. Atmos. Sci.*, **46,** 37–56.

Wang, B., and H. Rui, 1989: Some dynamic aspects of the equatorial intraseasonal oscillations. *East Asia and Western Pacific Meteorology and Climate.* P. Sham and C. P. Chang, Eds., World Scientific, 119–130.

——, and ——, 1990: Dynamics of the coupled moist Kelvin–Rossby wave on an equatorial β-plane. *J. Atmos. Sci.*, **47,** 397–413.